Acta Crystallographica Section D
Biological Crystallography
ISSN 1399-0047

Structural basis for the redox sensitivity of the *Mycobacterium tuberculosis* SigK–RskA σ–anti-σ complex

Jinal Shukla,[a] Radhika Gupta,[b] Krishan Gopal Thakur,[c] Rajesh Gokhale[b] and B. Gopal[a]*

[a]Molecular Biophysics Unit, Indian Institute of Science, Bangalore 560 012, India, [b]Institute of Genomics and Integrative Biology, New Delhi, India, and [c]Institute of Microbial Technology, Chandigarh, India

Correspondence e-mail: bgopal@mbu.iisc.ernet.in

Received 17 September 2013
Accepted 3 January 2014

PDB reference: SigK–RskA complex, 4nqw

The host–pathogen interactions in *Mycobacterium tuberculosis* infection are significantly influenced by redox stimuli and alterations in the levels of secreted antigens. The extracytoplasmic function (ECF) σ factor σ^{K} governs the transcription of the serodominant antigens MPT70 and MPT83. The cellular levels of σ^{K} are regulated by the membrane-associated anti-σ^{K} (RskA) that localizes σ^{K} in an inactive complex. The crystal structure of *M. tuberculosis* σ^{K} in complex with the cytosolic domain of RskA ($RskA_{cyto}$) revealed a disulfide bridge in the −35 promoter-interaction region of σ^{K}. Biochemical experiments reveal that the redox potential of the disulfide-forming cysteines in σ^{K} is consistent with its role as a sensor. The disulfide bond in σ^{K} influences the stability of the σ^{K}–$RskA_{cyto}$ complex but does not interfere with σ^{K}–promoter DNA interactions. It is noted that these disulfide-forming cysteines are conserved across homologues, suggesting that this could be a general mechanism for redox-sensitive transcription regulation.

1. Introduction

Mycobacterium tuberculosis encounters several diverse microenvironments in the host during the course of infection. An intriguing feature of this obligate aerobe is its ability to persist in a hypoxic microenvironment in the lungs. The mechanism that maintains redox homeostasis in *M. tuberculosis* under hypoxic conditions *in vivo* remains unclear. In addition to the cellular adaptation to redox stimuli, mycobacteria evade the host immune response by altering the levels of secreted antigenic proteins. These features present a significant challenge for the design of a new vaccine for tuberculosis. Indeed, the variable efficacy of the widely employed *M. bovis* Bacillus Calmette–Guérin (BCG) vaccine has been ascribed in part to differences in the response of *M. tuberculosis* and *M. bovis* to oxidative stimuli. For example, while CO_2 strongly inhibits the growth of *M. tuberculosis* both *in vitro* and *in vivo* (Dubos, 1953), low concentrations of CO_2 enhance the survival of *M. bovis* BCG under hypoxic conditions (Florczyk *et al.*, 2003).

Several pathogenic bacteria employ alternative σ factors to respond to changing microenvironments in the host during infection. These σ factors direct the RNA polymerase (RNAP) to specific promoters, thus influencing the expression profile of a bacterial cell. The extracytoplasmic function (ECF; also referred to as group IV) σ factors primarily regulate the cellular response to environmental stress (Helmann, 2002). The activity of these σ factors is regulated by their localization with anti-σ factors (Bashyam & Hasnain, 2004; Murakami *et al.*, 2002). The release of free σ factors from an inactive σ–anti-σ complex is achieved either by conformational

Table 1
Data-collection and structure-solution statistics (PDB entry 4nqw).

Values in parentheses are for the outer shell.

Diffraction source	Rigaku MicroMax-007 HF rotating-anode X-ray generator
Diffraction protocol	Single wavelength
Monochromator	VariMax HF
Wavelength (Å)	1.5418
Detector	MAR 345dtb
Temperature (K)	100
Resolution range (Å)	28.70–2.40 (2.53–2.40)
Total No. of reflections	144669 (22681)
No. of unique reflections	9747 (1480)
Completeness (%)	87.82 (100)
Multiplicity	14.8 (15.3)
$\langle I/\sigma(I)\rangle$	20.1 (8.1)
$R_{\rm merge}$†	0.09 (0.33)
CC*‡	0.998 (0.994)
Data-processing software	*MOSFLM*, *SCALA*

† $R_{\rm merge} = \sum_{hkl}\sum_i |I_i(hkl) - \langle I(hkl)\rangle| / \sum_{hkl}\sum_i I_i(hkl)$, where $I_i(hkl)$ is the intensity of the ith reflection and $\langle I(hkl)\rangle$ is the average intensity. ‡ Pearson correlation coefficient: $CC^* = [2CC_{1/2}/(1 + CC_{1/2})]^{1/2}$.

rearrangements or by selective proteolysis of the anti-σ factors (Urban, 2009; Lal & Caplan, 2011; Li *et al.*, 2009). Membrane-associated anti-σ factors often serve as sensors of environmental stimuli, thereby providing an effective mechanism that couples environmental changes to changes in gene expression.

$\sigma^{\rm K}$ (Rv0445c) is one of ten ECF σ-factors in *M. tuberculosis* and is negatively regulated by the anti-σ factor RskA. The $\sigma^{\rm K}$ regulon comprises of genes encoding $\sigma^{\rm K}$, RskA, UfaA1 (a cyclopropane-fatty-acyl phospholipid synthase), Rv0446c (a transmembrane protein with oxidoreductase activity), an aminooxidase (Rv0449c), DipZ (involved in cytochrome *c* biogenesis) and the secreted antigens MPT70 and MPT83 (Veyrier *et al.*, 2008). Recent studies have revealed that the expression of *katG*, a gene coding for catalase-peroxidase-peroxinitritase, is also regulated by $\sigma^{\rm K}$ (Sklar *et al.*, 2010). The $\sigma^{\rm K}$ regulon has been extensively examined in the context of the expression of MPT70 and MPT83 as these are important serodominant antigens during *M. bovis* infection, with defined T-cell responses in both mice and humans. Indeed, this finding led to the inclusion of MPT83 as an additional protective antigen in an antituberculosis vaccine directed at pulmonary tuberculosis (Kao *et al.*, 2012; Tyne *et al.*, 2013).

An unusual feature of the $\sigma^{\rm K}$ regulon is that despite extensive sequence conservation, the expression levels of the genes in this regulon vary widely across mycobacteria. This is particularly relevant from the perspective of host–pathogen interactions, as the expression levels of the immunogens MPT70 and MPT83 differ substantially between *M. tuberculosis* and *M. bovis* as well as between virulent and avirulent strains of *M. bovis* (Veyrier *et al.*, 2008; Kao *et al.*, 2012; Saïd-Salim *et al.*, 2006). These variations were ascribed to the anti-σ factor RskA, since a clear correlation was observed between the levels of antigen production and point mutations in *M. bovis* RskA (Chen *et al.*, 2012; Walzl *et al.*, 2011).

Here, we describe the mechanism by which the $\sigma^{\rm K}$–RskA complex synchronizes transcriptional changes with redox stimuli in *M. tuberculosis*. Previous reports suggested that RskA is a substrate for a proteolytic cascade initiated by site-1 and site-2 (Rv2869c) proteases (Makinoshima & Glickman, 2005; Sklar *et al.*, 2010). The concerted action of site-1 and site-2 proteases results in the dissociation of the cytosolic component (the $\sigma^{\rm K}$–$\rm RskA_{cyto}$ complex) from the membrane-bound RskA. The crystal structure and biochemical features of the $\sigma^{\rm K}$–$\rm RskA_{cyto}$ complex described here provide a basis for the rationalization of redox-dependent changes in the expression of the $\sigma^{\rm K}$ regulon. We demonstrate that the $\sigma^{\rm K}$–$\rm RskA_{cyto}$ complex dissociates under reducing conditions. The structure, biochemical studies and mutational analysis reveal that redox sensitivity is provided by cysteines involved in a disulfide bridge in the −35 promoter-binding region of $\sigma^{\rm K}$. The finding that $\sigma^{\rm K}$ could itself serve as a sensor for redox stimuli is the first such observation for a σ factor.

2. Materials and methods

2.1. Cloning, expression and purification

The details of the expression constructs used to obtain recombinant $\sigma^{\rm K}$, RskA (Rv0444c) and $\sigma^{\rm K}$–RskA-PhoA are summarized in Supplementary Table S1[1]. A single primer-based approach was employed to obtain cysteine-to-serine mutants of $\sigma^{\rm K}$. $\sigma^{\rm K}$–$\rm RskA_{cyto}$, $\sigma^{\rm K}$(C133S)–$\rm RskA_{cyto}$, $\sigma^{\rm K}$(C183S)–$\rm RskA_{cyto}$ and $\sigma^{\rm K}$(C133S,C183S)–$\rm RskA_{cyto}$ were purified by a co-expression and co-purification strategy. All of the proteins used in the biophysical experiments as well as in the crystallization trials were purified using the same protocol unless otherwise mentioned. *SigK* was cloned between the *Sac*I and *Not*I sites in the multiple cloning site 1 (MCS1) of the pETDuet1 expression vector. The gene encoding the cytosolic domain of RskA (amino acids 1–80) was cloned in MCS2 between the *Nde*I and *Kpn*I sites. The recombinant protein complex had a polyhistidine tag at the N-terminus of $\sigma^{\rm K}$. Residues Cys133 and Cys183 of $\sigma^{\rm K}$ were mutated to serines using the primers $\sigma^{\rm K}$(C133S), 5′-CGCCGGGTGACCGAGT-CCCTCAAGGCGTTGACC-3′, and $\sigma^{\rm K}$(C183S), 5′-GCAG-CCTGCGCAACTCCCTGGACGTGTCATGA-3′. The $\sigma^{\rm K}$–$\rm RskA_{cyto}$ constructs were transformed into *Escherichia coli* Rosetta(DE3) cells, which were grown at 37°C until an $\rm OD_{600}$ of 0.4 was obtained. Post induction with 0.3 m*M* isopropyl β-D-1-thiogalactopyranoside (IPTG), the cells were subsequently grown at 18°C for 12–14 h. The cells were harvested and resuspended in lysis buffer (50 m*M* Tris–HCl, 300 m*M* NaCl pH 8.0). The cell-free lysate was loaded onto a nickel-affinity column. The eluted fractions contained the recombinant protein complex, which could be concentrated to 10 mg $\rm ml^{-1}$ (Supplementary Table S1). The $\sigma^{\rm K}_4$ domain (123–187) was cloned between the *Bam*HI and *Hin*dIII sites in the pET-22b expression vector. The protein was purified by cation-exchange chromatography using SP Sepharose resin. The recombinant proteins were purified by size-exclusion chromatography for crystallization and fluorescence-anisotropy experiments.

[1] Supporting information has been deposited in the IUCr electronic archive (Reference: GM5029).

Table 2
Structure refinement and model validation.

Values in parentheses are for the outer shell.

Refinement software	*REFMAC* 5.7.0029
Resolution range (Å)	28.7–2.40
Completeness (%)	87.82
No. of reflections, working set	8305
No. of reflections, test set	916
Final R_{cryst}	0.21
Final R_{free}†	0.25
No. of non-H atoms	
Protein	1750
Ion	10
Ligand	0
Water	89
Total	1849
R.m.s. deviations	
Bonds (Å)	0.006
Angles (°)	1.04
Overall average *B* factor (Å^2)	32.80
Ramachandran plot analysis	
Most favoured regions (%)	100
Additionally allowed regions (%)	0
Disallowed regions (%)	0
Average *B* factors (Å^2)	
Chain *A*	
All atoms	34.97
Main chain	32.42
Side chain	37.46
Chain *B*	
All atoms	27.44
Main chain	25.90
Side chain	29.22
Water	35.66
Cd^{2+}	36.44
R.m.s.d. ΔB (bonded atoms) (Å^2)	
All protein atoms	2.59
Main chain–main chain	2.16
Side chain–side chain	2.84
Main chain–side chain	3.23
R.m.s.d. ΔB (non-bonded atoms) (Å^2)	6.69

† $R_{work} = \sum_{hkl} ||F_{obs}| - |F_{calc}|| / \sum_{hkl} |F_{obs}|$, where F_{calc} is the calculated protein structure factor from the atomic model. R_{free} was calculated as in the case of R_{work} but using 5% of the data, which were excluded from the refinement calculation (Brünger, 1992).

2.2. Analytical size-exclusion chromatography

For the size-exclusion chromatography experiments, ∼0.2–0.3 mg protein samples were passed through a Superdex S200 10/300 GL column (column volume 24 ml) equilibrated with 20 m*M* Tris–HCl pH 8.0, 200 m*M* NaCl at 6°C using a Bio-Rad (BioLogic DuoFlow) FPLC system. The elution profile was monitored by measuring the absorbance at 280 nm as well as at 220 nm. The flow rate was maintained at 0.3 ml min^{-1}. The σ^K–$RskA_{cyto}$ complex was subjected to reducing conditions by incubating the protein sample in a buffer consisting of 20 m*M* Tris–HCl pH 8.0, 200 m*M* NaCl with 5 m*M* TCEP as a reducing agent for 3 h.

2.3. Crystal structure determination

Crystallization trials for the σ^K–$RskA_{cyto}$ complex were performed using commercial screens (Hampton Research). The protein concentration varied from 5 to 30 mg ml^{-1} and the crystallization drops were set up by mixing 2 µl protein solution and 2 µl precipitant solution. Initial crystallization conditions (using a protein concentration of 5 mg ml^{-1}) were obtained in 0.1 *M* HEPES pH 7.5, 1 *M* sodium acetate trihydrate, 0.05 *M* cadmium sulfate hydrate using the microbatch method at 293 K. The crystallization conditions were further optimized using an additive screen (Hampton Research) to obtain diffraction-quality crystals. Crystals grown in the presence of 12%(*v*/*v*) 2,5-hexanediol were cryocooled to 100 K without further treatment; they belonged to space group $P4_12_12$ and diffracted to 2.4 Å resolution on a home source (MAR 345dtb image-plate detector mounted on a Rigaku MicroMax-007 HF rotating-anode X-ray generator). The diffraction data were processed using *iMosflm* (Battye *et al.*, 2011) and scaled using *SCALA* (Winn *et al.*, 2011). These data had a strong anomalous signal and the crystal structure was solved by single-wavelength anomalous dispersion (SAD) using the *AutoSol* module from the *PHENIX* software suite (Adams *et al.*, 2010). Ten heavy-atom sites were located with occupancies varying from 1 to 0.2. The initial model was built using the *AutoBuild* module in *PHENIX* (Adams *et al.*, 2010). Several rounds of manual model building using *Coot* (Emsley *et al.*, 2010) and refinement using *REFMAC*5 (Winn *et al.*, 2011) resulted in a model with final *R* and R_{free} values of 0.21 and 0.25, respectively (Brünger, 1992). The final model comprises residues 10–95 and 123–185 of σ^K and residues 7–79 of RskA. The linker (96–122) between σ^K_2 and σ^K_4 could not be modelled in the structure. The quality of the structural model was evaluated using *PROCHECK* (Laskowski *et al.*, 1993). The diffraction data and refinement statistics are compiled in Tables 1 and 2.

2.4. Circular-dichroism (CD) and thermostability measurements

The thermostability of the σ^K–$RskA_{cyto}$ complex was monitored by CD spectroscopy. The ellipticity measurements were recorded at 222 nm on a Jasco J-715 instrument. All spectra were recorded in 5 m*M* sodium phosphate buffer pH 7.5 using a 1 mm path-length cuvette. The protein concentration was maintained in the range 5–15 µ*M*. The temperature was varied from 20 to 85°C at a rate of 1°C per minute.

2.5. Redox-potential determination using intrinsic tryptophan fluorescence spectroscopy

Fluorescence-intensity measurements were performed using the σ^K–$RskA_{cyto}$ complex at 2–4 µ*M* in a buffer consisting of 10 m*M* HEPES pH 7.5 at room temperature. The excitation wavelength was set to 280 nm, while the emission spectra were recorded from 300 to 400 nm at a bandwidth of 1 nm. Each recorded spectrum represents an average of three scans. The spectra for the oxidized, reduced and denatured forms of protein were recorded after incubating the protein in either 1 m*M* H_2O_2, 10 m*M* DTT or 6 *M* guanidine–HCl for 10 min prior to the experiment.

The redox potential of the disulfide-forming cysteines in σ^K was estimated using the GSH/GSSG redox couple. For the determination of the equilibrium constants of the σ^K–$RskA_{cyto}$/glutathione redox system, freshly prepared protein samples (4 µ*M*) were incubated at 4°C in the presence of

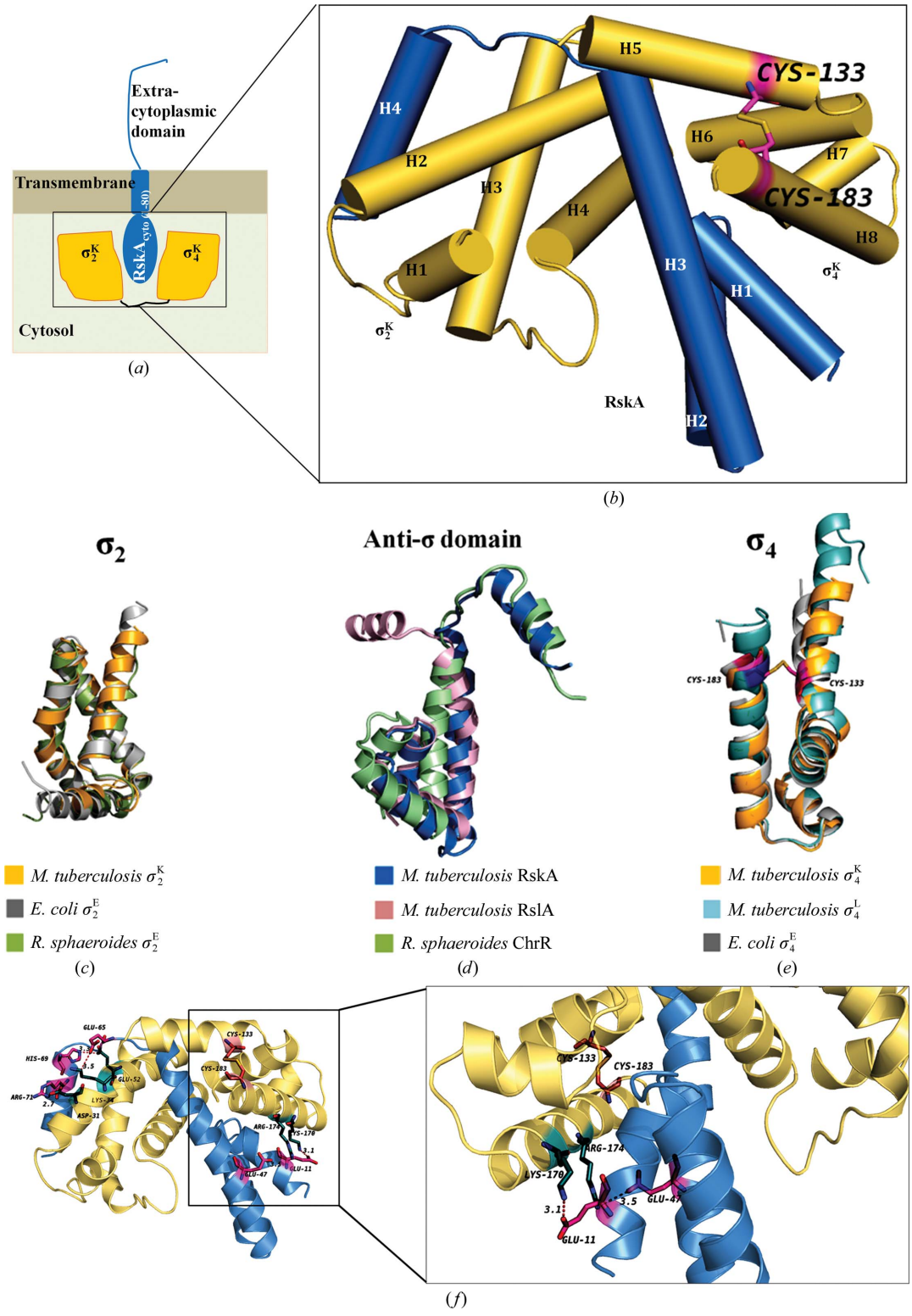

Figure 1
Crystal structure of *M. tuberculosis* σ^{K} in complex with its negative regulator RskA. (*a*) The transmembrane anti-σ factor RskA negatively regulates and localizes *M. tuberculosis* σ^{K}. (*b*) The crystal structure of σ^{K} (yellow) in complex with the cytosolic anti-σ domain of RskA (blue) reveals that RskA binding occludes the RNA polymerase interacting and DNA-binding surfaces of σ^{K}. The crystal structure reveals a disulfide in domain 4 of σ^{K}. (*c*) Superposition of σ_2^{K} on *E. coli* σ_2^{E} (structure obtained from the *E. coli* σ^{E}–RsrA complex; PDB entry 1or7; Campbell *et al.*, 2003) and *R. sphaeroides* σ_2^{E} (from the *R. sphaeroides* σ^{E}–ChrR complex; PDB entry 2z2s; Campbell *et al.*, 2007). (*d*) Superposition of the ASDs of *M. tuberculosis* RskA and RslA (Thakur *et al.*, 2010) on the ASD of *R. sphaeroides* ChrR (Campbell *et al.*, 2007). (*e*) Superposition of σ_4^{K} on σ_4^{E} of *R. sphaeroides* (PDB entry 2z2s; Campbell *et al.*, 2007) and *M. tuberculosis* σ_4^{L} (structure obtained from the *M. tuberculosis* σ_4^{L}–RslA complex; PDB entry 3hug; Thakur *et al.*, 2010). (*f*) The σ^{K}–RskA$_{cyto}$ complex reveals extensive interactions between the structured domains of σ^{K} and RskA$_{cyto}$ that effectively occlude the DNA-binding and RNA polymerase interacting regions of σ^{K}. This interface mostly involves van der Waals interactions, with few polar interactions.

0.01 m*M* GSSG. The concentration of GSH was varied from 30 to 95 m*M*. Equilibration of the protein at constant GSSG but varying GSH concentrations was achieved using a standard Schlenk-line technique under anaerobic conditions (McLlwrick & Phillips, 1973). An anaerobic environment was maintained using a constant flow of argon throughout the reaction setup (incubation time of 90 min at pH7.5). All of the samples and buffers were flushed with argon to exclude air oxidation. The equilibrium concentrations of GSH and GSSG were calculated according to (1)–(3), where $[GSH]_0$ and $[GSSG]_0$ are the initial concentrations of GSH and GSSG, respectively, R is the relative amount of reduced protein at equilibrium and $[P]_0$ is the initial concentration of the oxidized form of σ^K–RskA$_{cyto}$. In this formalism, F_i is the measured fluorescence intensity, while F_{ox} and F_{red} are the fluorescence intensities of the completely oxidized and reduced forms of the protein, respectively (Wunderlich & Glockshuber, 1993).

$$[GSH] = [GSH]_0 - 2R[P]_0, \quad (1)$$

$$[GSSG] = [GSSG]_0 + R[P]_0, \quad (2)$$

$$R = (F_i - F_{ox})/(F_{red} - F_{ox}), \quad (3)$$

$$R = \frac{[GSH]^2/[GSSG]}{K_{eq} + [GSH]^2/[GSSG]}, \quad (4)$$

$$E_0(\sigma^K/RskA) = E_0(GSH/GSSG) - (RT/nF)\ln K_{eq}. \quad (5)$$

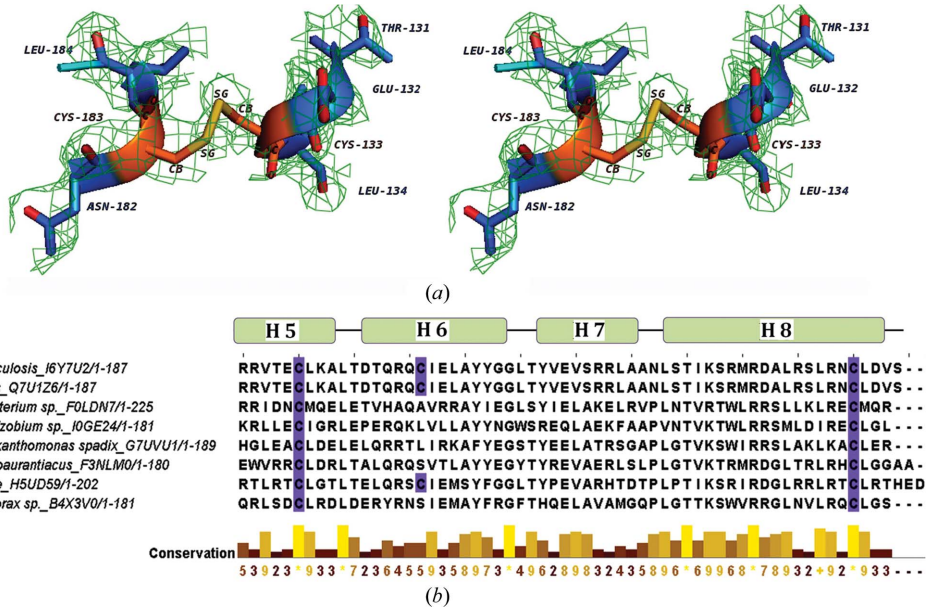

Figure 2
The σ^K–RskA$_{cyto}$ complex reveals a disulfide bond in the −35 promoter-binding region of σ^K. (*a*) A stereoview of the experimental electron-density map (contoured at 1.0σ) showing the disulfide bridge between Cys133 and Cys183 in σ^K_4. All structural images were prepared using *PyMOL* (v.1.2r3pre; Schrödinger). (*b*) Multiple sequence alignment of σ^K with its homologues. In this set of sequences (sequence identity >27%), the cysteines involved in the disulfide bond are conserved (Supplementary Fig. S2).

Table 3
Dissociation constant (K_d) for σ^K–RskA$_{cyto}$ interactions.

Condition	K_d (μ*M*)
Oxidized σ^K	0.42 ± 0.05
Reduced σ^K	1.15 ± 0.12

The data were fitted to (4) with a correlation coefficient of 0.97. The redox potential was then calculated from the Nernst equation using the standard glutathione potential (5) (Fig. 3).

2.6. Surface plasmon resonance measurements

The interaction between the oxidized and reduced forms of σ^K and RskA$_{cyto}$ was examined using surface plasmon resonance (Biacore 3000; GE Healthcare). Reduced σ^K was obtained by incubating the protein in 1 m*M* TCEP for 2 h. RskA$_{cyto}$ was immobilized on a CM5 chip (Biacore; GE Healthcare) at a surface density of 12 ng mm^{-2}. The interaction kinetics were evaluated using the *BIAevaluation* software [the dissociation constants compiled in Table 3 include the calculated standard error of mean (SEM)]. The first lane of the chip was used as a control and all of the interactions were examined in a buffer consisting of 20 m*M* HEPES, 100 m*M* NaCl pH 7.6.

2.7. Fluorescence anisotropy

The oligonucleotide primers for fluorescence-aniosotropy experiments were designed based on the −35 promoter DNA element preceding the *mpt70* and *katG* genes (Supplementary Fig. S6). These oligomers were labelled with 6-carboxy fluorescein (6-FAM) at the 3′ end. 10 n*M* of the −35 promoter DNA was incubated with increasing concentrations of σ^K_4 (0.5–300 n*M*, with 1 m*M* TCEP for reducing conditions) in the dark for 20 min. The reaction was set up in a 96-well ELISA plate. The emission was measured at 520 nm and the $I_{\parallel}$ and $I_{\perp}$ values were recorded. The anisotropy measurements were fitted to a sigmoidal curve to obtain the dissociation constant (K_d).

3. Results

3.1. Crystal structure of the σ^K–RskA$_{cyto}$ complex

Crystals of σ^K in complex with the anti-σ domain (RskA$_{cyto}$) diffracted to a Bragg spacing (d_{min}) of 2.4 Å (Figs. 1*a* and 1*b*). The crystal structure was solved by the single-wavelength anomalous dispersion (SAD) method

using the anomalous signal of the bound Cd atoms (Tables 1 and 2; PDB entry 4nqw). The bound Cd^{2+} ions could be ascribed to the crystallization buffer and are not likely to be physiologically relevant. There are ten Cd^{2+} ions bound to residues on the surface, mainly to Asp, Glu, His and Cys residues. In most cases, the coordination number for the bound ion is either four or five, with water molecules completing the coordination geometry. Consistent with the previous analyses, the preference for amino acids coordinating the Cd^{2+} ions is Glu > Asp > His > Cys (Jesu Jaya Sudan & Sudandiradoss, 2012; Harding, 2004, 2006). The bound Cd^{2+} ions contribute to crystal packing. Six of the ten Cd^{2+} ions share protein ligands from the neighbouring symmetry mates.

σ^K has two structured domains (referred to as region 2 and region 4; σ_2^K and σ_4^K, respectively) connected by a flexible linker (Figs. 1*a* and 1*b*). Both domains superpose well with the corresponding domains of other σ factors (Figs. 1*c* and 1*e* and Supplementary Table S2). The Pribnow box recognition domain (σ_2^K) adopts an antiparallel three-helical bundle structure. As in other σ_2 domains, helix H1 in σ_2^K is the longest. A 45° kink that occurs midway in helix H1 of domain 2 distinguishes σ_2^K from eukaryotic transcription factors that adopt a similar conformation (Li *et al.*, 2002).

$RskA_{cyto}$ has the canonical anti-σ domain (ASD) fold, a structural module first seen in the *Rhodobacter sphaeroides* σ^E–ChrR complex (Campbell *et al.*, 2007). While the ASDs of *R. sphaeroides* ChrR and *M. tuberculosis* $RskA_{cyto}$ share only 9.2% sequence identity, they superpose well with a r.m.s.d. of 1.9 Å over 65 C^α positions (Supplementary Table S2; Fig. 1*d*). As in the case of the structured domains of σ factors, poor

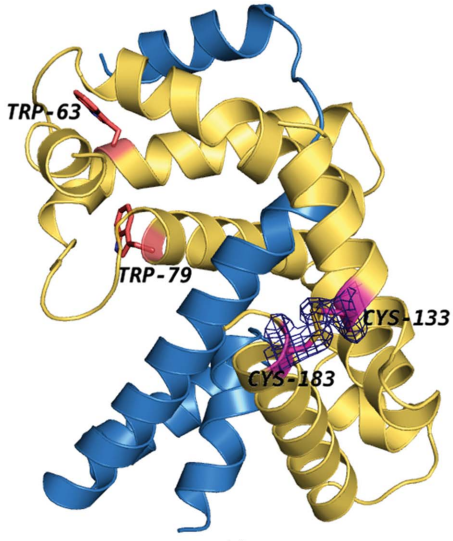

(*a*)

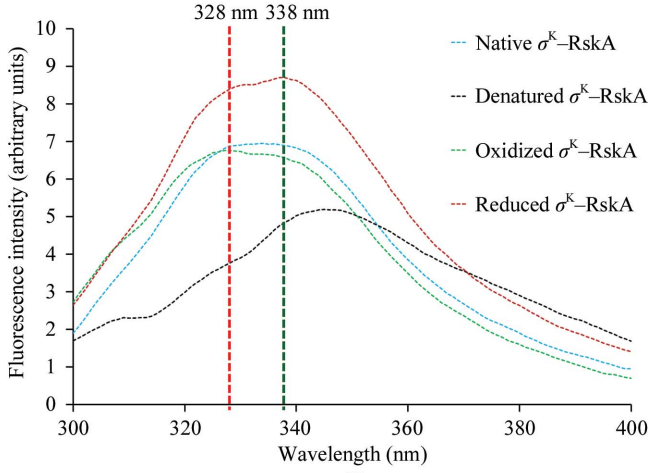

(*b*)

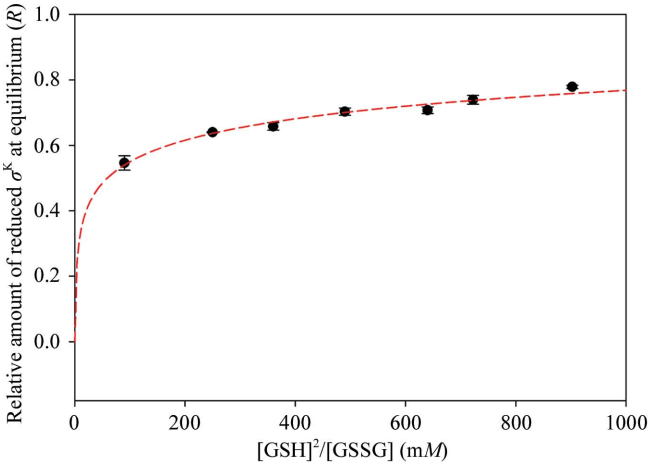

(*c*)

$[GSH]^2/[GSSG]$ (m*M*)	K_{eq} (*M*)	E_o (mV)
90	0.065	−275
250	0.110	−268
360	0.150	−264
490	0.155	−264
640	0.198	−261
722.5	0.207	−260
902.5	0.191	−261
	Mean K_{eq} (*M*)	0.1475
	Mean E_o (mV)	−265

(*d*)

Figure 3
A disulfide bond in the −35 promoter-binding domain of σ^K acts as a redox sensor. (*a*) The experimental electron-density map at 2.4 Å resolution (1.0σ level) reveals a disulfide between Cys133 of helix H5 and Cys183 of helix H8 in the σ_4^K domain. (*b*) Intrinsic tryptophan fluorescence was monitored from 300 to 400 nm for freshly purified σ^K–$RskA_{cyto}$ as well as the oxidized, reduced and denatured protein samples. These spectra reveal a 10 nm shift between the oxidized and reduced samples. The oxidized and reduced forms of the cysteine residues in σ^K were confirmed by mass spectrometry (Supplementary Fig. S1). (*c*) The redox potential was measured with a glutathione-coupled assay using the intrinsic tryptophan fluorescence of this protein (Wunderlich & Glockshuber, 1993). The plot shows the amount of σ^K–$RskA_{cyto}$ complex equilibrated with varying concentrations of GSH. (*d*) The K_{eq} calculated for the σ^K–$RskA_{cyto}$ complex at different ratios of $[GSH]^2/GSSG$ was used in the Nernst equation to calculate the redox potential. The mean redox potential of −265 mV for the σ^K–$RskA_{cyto}$ complex suggests the cysteines are likely to be oxidized in the cytosolic environment.

sequence similarity between different ASDs belies the underlying structural conservation. Indeed, a structure-based sequence analysis was crucial to identify this structurally conserved component in different anti-σ factors (Campbell *et al.*, 2007). Of the four helices in $RskA_{cyto}$, the three N-terminal helices form a compact structure. Helix H4 adopts a different orientation with respect to the three-helical N-terminal domain in $RskA_{cyto}$. When the ASDs of RskA and RslA (from the *M. tuberculosis* σ^{L}_{4}–RslA complex; PDB entry 3hug; Thakur *et al.*, 2010) are superposed, they show distinctly different orientations of helix H4 (Fig. 1*d*). The σ^{K}–$RskA_{cyto}$ complex reveals extensive interactions between the structured domains of σ^{K} and $RskA_{cyto}$ that effectively occlude the DNA-binding and RNA polymerase interacting regions of σ^{K} (Murakami, 2013). This interface mostly involves van der Waals interactions, with few polar interactions. The most prominent amongst the polar interactions are those between Lys170, Arg174, Lys34 and Asp31 of σ^{K} with Glu11, Glu47, Glu65 and Arg71 of RskA (Fig. 1*f*). Both σ^{K}_{2} and σ^{K}_{4} make a similar number of contacts with $RskA_{cyto}$, involving a buried surface area of 2047 Å^{2} (Supplementary Table S3, Fig. 1*f*; Krissinel & Henrick, 2007). It is worth noting in this context that the relative roles of the σ_2 and σ_4 domains in different σ–anti-σ complexes vary, perhaps influencing the binding affinity between the σ factor and the corresponding ASD. While σ_4 plays a prominent role in *B. subtilis* σ^{F} and *Salmonella typhimurium* σ^{28}, σ_2 dominates in the case of the *S. coelicolor* σ^{R}–RsrA complex. This observation was also substantiated by biochemical data in the case of the *S. coelicolor* σ^{R}–RsrA interactions. Indeed, a σ^{R} polypeptide segment containing σ^{R}_{4} did not interact with the ASD of RsrA in solution (Li *et al.*, 2002)

3.2. Conserved cysteines in σ^{K}_{4} form a disulfide bond

The experimental electron-density map of the σ^{K}–$RskA_{cyto}$ complex revealed a disulfide bond between Cys133 and Cys183 in the −35 promoter-binding domain (σ^{K}_{4}; Fig. 2*a*). This finding is consistent with mass-spectrometric analysis of freshly purified σ^{K}/$RskA_{cyto}$ protein samples (Supplementary Fig. S1). This unexpected finding of a disulfide prompted a re-examination of σ-factor sequences. Multiple sequence alignment (using 212 sequences sharing sequence identity better than 27%) revealed that these Cys residues are conserved in

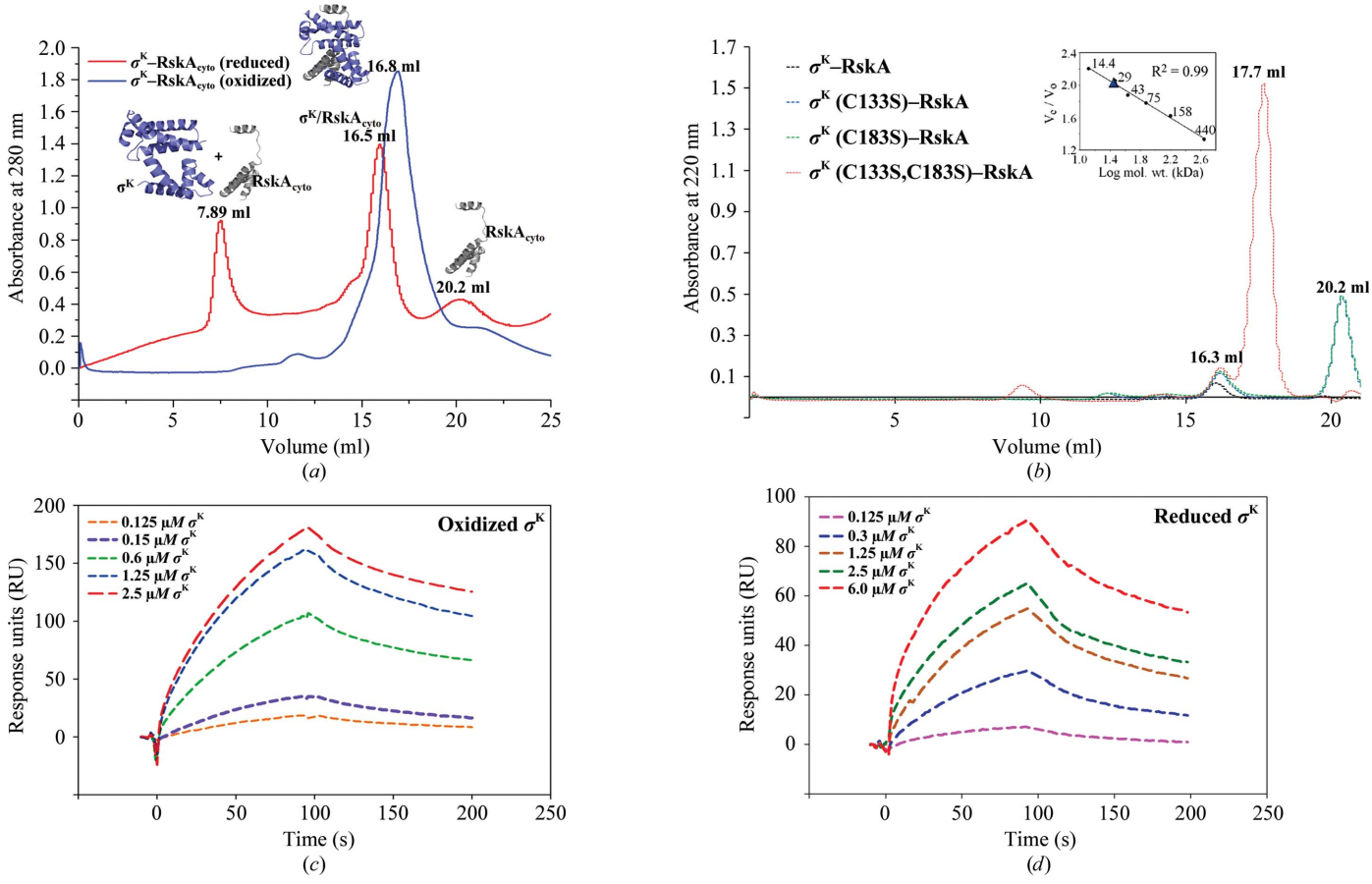

Figure 4
The disulfide in σ^{K} influences σ^{K}–$RskA_{cyto}$ interactions. (*a*) Comparison of analytical size-exclusion chromatography profiles of the σ^{K}–$RskA_{cyto}$ complex in the presence and absence of a reducing agent. Mass spectra of the eluant (peak corresponding to 20.2 ml) are shown in Supplementary Fig. S3. (*b*) Analytical size-exclusion profile for wild-type σ^{K}–$RskA_{cyto}$ and the σ^{K}(C133S)–$RskA_{cyto}$, σ^{K}(C183S)–$RskA_{cyto}$ and σ^{K}(C133S,C183S)–$RskA_{cyto}$ mutants. The peak at 17.7 ml was identified as σ^{K}(C133S,C183S) using LC-MS data (Supplementary Fig. S4). (*c*, *d*) The dissociation constant (K_d) between σ^{K} and $RskA_{cyto}$ was determined by surface plasmon resonance (SPR). Analysis of the SPR sensograms reveals a threefold increase in the dissociation constant between σ^{K} and $RskA_{cyto}$ in the presence of a reducing agent (1 m*M* TCEP).

~70% of these sequences, which included 60% from Gram-positive and 40% from Gram-negative bacteria (Fig. 2*b*, Supplementary Fig. S2 and Supporting Information). These cysteines are conserved in σ^{K} homologues from 67 different bacterial species. While this included 21 mycobacterial proteins, a majority of the homologues are from *Streptomyces* (27 protein sequences). We note that σ^{K} homologues are mostly found in *Actinobacteria* followed by the proteobacterial species (alphaproteobacteria > gammaproteobacteria > betaproteobacteria). The co-occurrence of these disulfide-forming cysteines suggested that the disulfide bond is likely to be conserved in these σ factors (Figs. 2*a*, 2*b* and Supplementary Fig. S2).

3.3. The redox potential of the disulfide-forming cysteines in σ_4^{K}

The disulfide in σ_4^{K} (the first such observation for a σ factor) prompted us to evaluate the role of this disulfide in σ^{K}–$RskA_{cyto}$ interactions. The redox potential of the disulfide-forming cysteines in σ^{K} was examined by fluorescence spectroscopy. These experiments, which were performed using intrinsic tryptophan fluorescence, were aided by the changes in the fluorescence spectra between the oxidized and reduced forms of σ^{K}. There are two tryptophan residues in σ^{K}. $RskA_{cyto}$ does not contain any tryptophan residues (Fig. 3*a*). A blue shift in the emission spectra (10 nm) along with a decrease in the relative fluorescence intensity was observed for the oxidized σ^{K}–$RskA_{cyto}$ complex when compared with the reduced form (Fig. 3*b*). These spectral changes allowed us to evaluate the redox potential of the cysteines using the standard glutathione redox (GSH/GSSG) couple. These fluorescence experiments, in which the σ^{K}–$RskA_{cyto}$ sample was equilibrated with varying concentrations of reduced glutathione at a fixed concentration of oxidized glutathione at pH 7.5, suggested an equilibrium constant of 14×10^{-2} *M*. This corresponds to a redox potential E_0' (calculated using the Nernst equation) of −0.265 V (Figs. 3*c* and 3*d*). This redox potential is similar to the well characterized redox-sensor protein thioredoxin as well as *E. coli* DsbB (Regeimbal & Bardwell, 2002; Sevier & Kaiser, 2002; Stewart *et al.*, 1998).

3.4. The disulfide contributes to the stability of the σ^{K}–$RskA_{cyto}$ complex

The σ^{K}–$RskA_{cyto}$ complex adopts a 1:1 stoichiometry in solution. The freshly purified protein complex elutes as a single peak corresponding to the σ^{K}–$RskA_{cyto}$ heterodimer

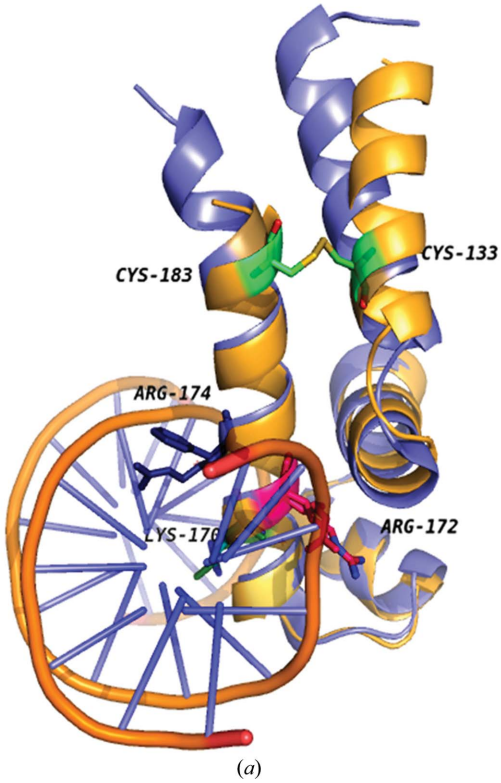

(*a*)

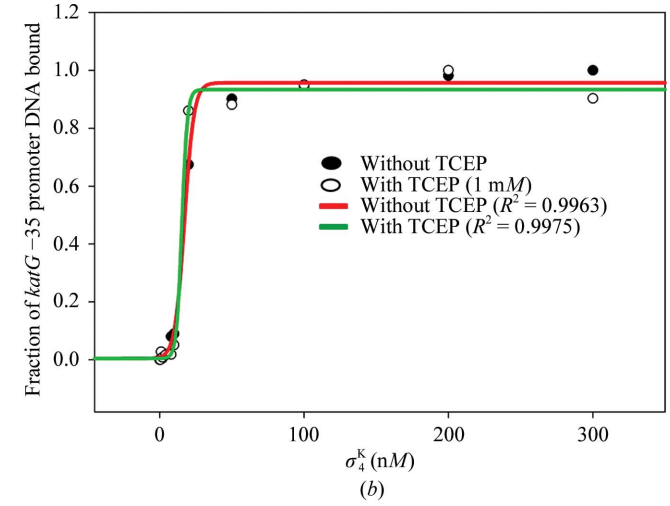

(*b*)

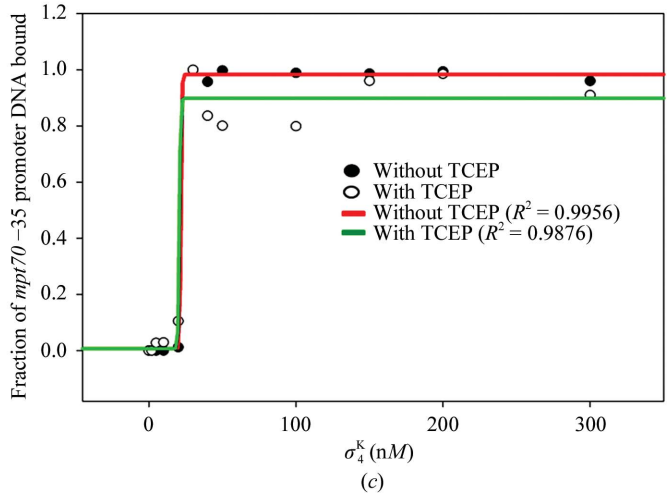

(*c*)

Figure 5
The disulfide bridge does not affect σ^{K}–promoter interactions. (*a*) Superposition of σ_4^{K} (yellow) on *E. coli* σ_4^{E} in complex with the −35 promoter-element DNA (PDB entry 2h27; blue). (*b*, *c*) Data from the fluorescence-anisotropy measurements in the absence (red) and presence (green) of 1 m*M* TCEP are shown as the fraction of the promoter DNA bound to σ_4^{K}. The binding affinities of σ_4^{K} for two representative −35 promoter-elements DNA (*katG* and *mpt70*) were examined.

in an analytical size-exclusion experiment (Fig. 4*a*). Under reducing conditions, $RskA_{cyto}$ was observed to dissociate from the σ^K–$RskA_{cyto}$ complex. This is evident from the elution profile, in which the single peak corresponding to the σ^K–$RskA_{cyto}$ complex is replaced by a smaller peak at 20.2 ml (corresponding to $RskA_{cyto}$) alongside the σ^K–$RskA_{cyto}$ complex (7.98 ml). The identity of the protein samples corresponding to these elution profiles were confirmed using electrospray ionization mass spectrometry (Supplementary Fig. S3). This observation on σ^K–$RskA_{cyto}$ samples under reducing conditions was consistent with the solution behaviour of a mutant σ^K–$RskA_{cyto}$ complex in which the cysteine residues involved in the disulfide bond in σ^K were mutated to serines (Fig. 4*b* and Supplementary Fig. S4). The disulfide in σ^K_4 also contributes substantially to the stability of the σ^K–RskA complex. Thermal denaturation experiments reveal that the T_m reduces by ~10°C upon mutating either or both of these cysteine residues (Supplementary Fig. S5). The interaction affinity between σ^K and $RskA_{cyto}$ under ambient as well as reducing conditions was determined by surface plasmon resonance (SPR) experiments. Analysis of the SPR sensograms revealed that the dissociation constant K_d corresponding to the oxidized σ^K–$RskA_{cyto}$ complex was ~0.4 μ*M*. A threefold increase in K_d was noted when σ^K and $RskA_{cyto}$ were made to interact under reducing conditions (~1.15 μ*M*; Figs. 4*c* and 4*d*, Table 3).

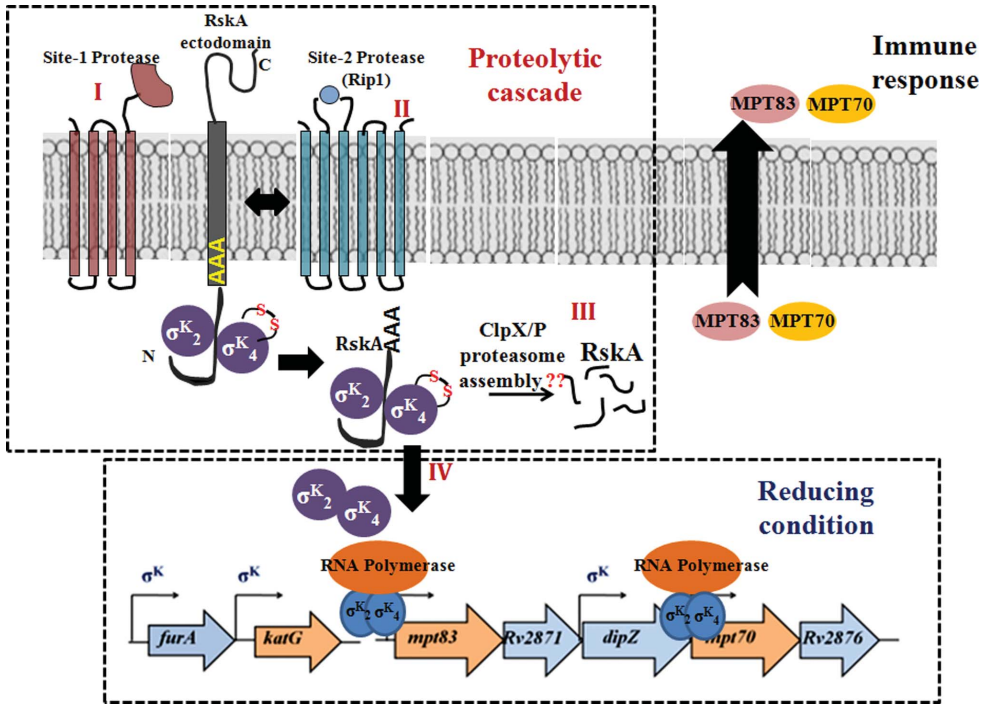

Figure 6
Multiple regulatory steps govern the cellular concentration of *M. tuberculosis* σ^K. A mechanistic model placing the redox-sensitive activation of σ^K in the context of the partially characterized regulated proteolytic cascade that governs the intracellular levels of σ^K. Transmembrane signalling in RskA is governed by the proteolysis of the ectodomain by a site-1 protease (I) that serves as a trigger for a site-2 protease (Rip1 in the case of RskA) activity (II) (Makinoshima & Glickman, 2005; Urban, 2009; Sklar *et al.*, 2010). Exposed sequence and/or structural motifs potentially lead to the selective degradation of the cytosolic RskA (Li *et al.*, 2009; Lal & Caplan, 2011) (III). Reducing conditions substantially weaken σ^K–$RskA_{cyto}$ interactions owing to the reduction of the disulfide in σ^K_4 (IV) (this study). Free, transcriptionally active σ^K enhances the expression of genes involved in the regulation of redox homeostasis and serodominant antigens (Sklar *et al.*, 2010).

3.5. The disulfide bond in σ^K_4 does not affect promoter interactions

The structural similarity of the −35 element recognition domain, σ^K_4, to the σ_4 domain of *Thermus aquaticus* σ^A (in complex with −35 element DNA) and *E. coli* σ^E_4 (also in complex with the −35 promoter-element DNA) suggested that the conformation of this domain was well conserved, with an overall r.m.s.d. of 0.78 Å over 55 C^α atoms. Residues involved in promoter DNA interactions, in particular, superpose well, suggesting that the disulfide does not alter the conformation of the helix–turn–helix motif (Campbell *et al.*, 2002; Lane & Darst, 2006; Fig. 5*a*). It thus appeared likely that the role of the disulfide would be restricted to redox-sensitive σ^K–$RskA_{cyto}$ interactions and that it would have no role in σ^K_4–DNA interactions. Fluorescence-anisotropy experiments were performed to evaluate the binding affinities of σ^K_4 for the −35 promoter element of *katG* and *mpt70* in the presence and absence of a reducing agent (Supplementary Fig. S6). Both of these genes are regulated by σ^K. The binding affinities of σ^K_4 to both the −35 promoter DNA elements were similar under ambient and reducing conditions (Figs. 5*b* and 5*c* and Supplementary Table S4). Put together, the biochemical data suggest that the disulfide influences σ^K–$RskA_{cyto}$ interactions and does not affect promoter DNA binding.

4. Discussion

The finding that *M. tuberculosis* σ^K–RskA interactions are affected by redox stimuli is a feature that is likely to be conserved across other ECF σ factors. An alignment of σ-factor sequences revealed that the disulfide-forming cysteine residues were conserved in the vast majority (70%) of the sequences that were examined. This finding suggests a variation of the well characterized model for σ factor–anti-σ factor interactions in which the environmental sensor is located in the anti-σ factor. Examples of this mechanism include the *Streptomyces coelicolor* σ^R–RsrA complex, in

which a disulfide in the anti-σ factor (RsrA) is responsive to redox stimuli (Li *et al.*, 2002). The anti-σ factor also serves as a sensor in the *R. sphaeroides* σ^{E}–ChrR complex as well as the *M. tuberculosis* σ^{L}–RslA complex. The anti-σ factors in these cases contain a C*XX*C motif that binds Zn^{2+}. In *M. tuberculosis* RslA, removal of the bound Zn^{2+} ion precedes the formation of a disulfide under oxidizing conditions (Campbell *et al.*, 2007; Thakur *et al.*, 2010). The regulator of an anti-σ factor (anti-anti-σ) can also adopt the role of a redox sensor. An example of this mechanism is the *Bacillus subtilis* σ^{F}–UsfX σ–anti-σ complex. A disulfide bond in the anti-anti-σ factor RsfA mediates redox-sensitive RsfA–UsfX interactions (Malik *et al.*, 2009).

An important feature that distinguishes the redox sensor in σ^{K} from other redox-sensitive transcriptional regulators is that the disulfide does not affect protein–DNA interactions. In the case of *S. aureus* AgrA (a two-component response regulator that governs quorum sensing), for example, the disulfide abrogates DNA binding (Sun *et al.*, 2012). The redox sensor in σ^{K} is thus a positive regulator that can increase the intracellular levels of σ^{K} under reducing conditions. The redox sensitivity of the σ^{K}–$RskA_{cyto}$ complex acquires further significance in the context of the sensitivity of site-1 and site-2 proteases to redox stimuli (Sklar *et al.*, 2010). The synchronized action of these proteases is essential for the dissociation of the σ^{K}–$RskA_{cyto}$ complex from the membrane.

It is likely that the response of the *M. tuberculosis* σ^{K}–RskA complex to environmental stimuli is regulated by multiple mechanisms (Fig. 6). One potential regulatory mechanism could involve modulation of the activity of the site-1 protease that cleaves RskA and initiates signalling in response to environmental stimuli. This step is essential to trigger site-2 cleavage by the site-2 protease (Urban, 2009; Sklar *et al.*, 2010). The σ^{K}–$RskA_{cyto}$ complex, on the other hand, dissociates under reducing conditions to activate σ^{K}. This multilayered regulatory system reveals an exquisite mechanism in *M. tuberculosis* to couple redox responses to changes in the levels of secreted antigenic proteins. This ability to coordinate a cellular response to the host innate and acquired immune system perhaps explains the persistence of this bacillus under unfavourable microenvironments in the host for extended periods of time.

5. Concluding remarks

A disulfide in the −35 promoter-binding domain of σ^{K} influences σ^{K}–$RskA_{cyto}$ interactions. The redox potential of the disulfide-forming cysteine residues is consistent with its role as a redox sensor. The disulfide-forming cysteine residues are conserved across homologues. The redox sensitivity of σ^{K}–$RskA_{cyto}$ interactions is thus likely to be a general feature across homologous σ–anti-σ complexes, potentially influencing redox-sensitive transcription regulation.

This work was supported by a grant from the Department of Biotechnology, Government of India. We thank Professor Balaji Jagirdar and Mr Ramaraj A for their advice and support in setting up the Schlenk manifold for the redox-1potential measurements.

References

Adams, P. D. *et al.* (2010). *Acta Cryst.* D**66**, 213–221.
Bashyam, M. D. & Hasnain, S. E. (2004). *Infect. Genet. Evol.* **4**, 301–308.
Battye, T. G. G., Kontogiannis, L., Johnson, O., Powell, H. R. & Leslie, A. G. W. (2011). *Acta Cryst.* D**67**, 271–281.
Brünger, A. T. (1992). *Nature (London)*, **355**, 472–475.
Campbell, E. A., Greenwell, R., Anthony, J. R., Wang, S., Lim, L., Das, K., Sofia, H. J., Donohue, T. J. & Darst, S. A. (2007). *Mol. Cell*, **27**, 793–805.
Campbell, E. A., Muzzin, O., Chlenov, M., Sun, J. L., Olson, C. A., Weinman, O., Trester-Zedlitz, M. L. & Darst, S. A. (2002). *Mol. Cell*, **9**, 527–539.
Campbell, E. A., Tupy, J. L., Gruber, T. M., Wang, S., Sharp, M. M., Gross, C. A. & Darst, S. A. (2003). *Mol. Cell*, **11**, 1067–1078.
Chen, S.-T., Li, J.-Y., Zhang, Y., Gao, X. & Cai, H. (2012). *J. Immunol.* **188**, 668–677.
Dubos, R. J. (1953). *J. Exp. Med.* **97**, 357–366.
Emsley, P., Lohkamp, B., Scott, W. G. & Cowtan, K. (2010). *Acta Cryst.* D**66**, 486–501.
Florczyk, M. A., McCue, L. A., Purkayastha, A., Currenti, E., Wolin, M. J. & McDonough, K. A. (2003). *Infect. Immun.* **71**, 5332–5343.
Harding, M. M. (2004). *Acta Cryst.* D**60**, 849–859.
Harding, M. M. (2006). *Acta Cryst.* D**62**, 678–682.
Helmann, J. D. (2002). *Adv. Microb. Physiol.* **46**, 47–110.
Jesu Jaya Sudan, R. & Sudandiradoss, C. (2012). *Acta Cryst.* D**68**, 1346–1358.
Kao, F. F., Mahmuda, S., Pinto, R., Triccas, J. A., West, N. P. & Britton, W. J. (2012). *PLoS One*, **7**, e34991.
Krissinel, E. & Henrick, K. (2007). *J. Mol. Biol.* **372**, 774–797.
Lal, M. & Caplan, M. (2011). *Physiology*, **26**, 34–44.
Lane, W. J. & Darst, S. A. (2006). *PLoS Biol.* **4**, e269.
Laskowski, R. A., MacArthur, M. W., Moss, D. S. & Thornton, J. M. (1993). *J. Appl. Cryst.* **26**, 283–291.
Li, W., Stevenson, C. E., Burton, N., Jakimowicz, P., Paget, M. S., Buttner, M. J., Lawson, D. M. & Kleanthous, C. (2002). *J. Mol. Biol.* **323**, 225–236.
Li, X., Wang, B., Feng, L., Kang, H., Qi, Y., Wang, J. & Shi, Y. (2009). *Proc. Natl Acad. Sci. USA*, **106**, 14837–14842.
Makinoshima, H. & Glickman, M. S. (2005). *Nature (London)*, **436**, 406–409.
Malik, S. S., Luthra, A. & Ramachandran, R. (2009). *Biochim. Biophys. Acta*, **1794**, 541–553.
McLlwrick, C. R. & Phillips, C. S. (1973). *J. Phys. E*, **6**, 1208–1210.
Murakami, K. S. (2013). *J. Biol. Chem.* **288**, 9126–9134.
Murakami, K. S., Masuda, S. & Darst, S. A. (2002). *Science*, **296**, 1280–1284.
Regeimbal, J. & Bardwell, J. C. (2002). *J. Biol. Chem.* **277**, 32706–32713.
Saïd-Salim, B., Mostowy, S., Kristof, A. S. & Behr, M. A. (2006). *Mol. Microbiol.* **62**, 1251–1263.
Sevier, C. S. & Kaiser, C. A. (2002). *Nature Rev. Mol. Cell Biol.* **3**, 836–847.
Sklar, J. G., Makinoshima, H., Schneider, J. S. & Glickman, M. S. (2010). *Mol. Microbiol.* **77**, 605–617.
Stewart, E. J., Aslund, F. & Beckwith, J. (1998). *EMBO J.* **17**, 5543–5550.
Sun, F., Liang, H., Kong, X., Xie, S., Cho, H., Deng, X., Ji, Q., Zhang, H., Alvarez, S., Hicks, L. M., Bae, T., Luo, C., Jiang, H. & He, C. (2012). *Proc. Natl Acad. Sci. USA*, **109**, 9095–9100.
Thakur, K. G., Praveena, T. & Gopal, B. (2010). *J. Mol. Biol.* **397**, 1199–1208.
Tyne, A. S., Chan, J. G. Y., Shanahan, E. R., Atmosukarto, I., Chan, H.-K., Britton, W. J. & West, N. P. (2013). *Vaccine*, **31**, 4322–4329.

Urban, S. (2009). *Nature Rev. Microbiol.* **7**, 411–423.
Veyrier, F., Saïd-Salim, B. & Behr, M. A. (2008). *J. Bacteriol.* **190**, 1891–1899.
Walzl, G., Ronacher, K., Hanekom, W., Scriba, T. J. & Zumla, A. (2011). *Nature Rev. Immunol.* **11**, 343–354.
Winn, M. D. *et al.* (2011). *Acta Cryst.* D**67**, 235–242.
Wunderlich, M. & Glockshuber, R. (1993). *Protein Sci.* **2**, 717–726.